Quantum Sensing of Thermoreflectivity in Electronics

Hamza Ather,[1,2] Haechan An,[1] Hal Owens,[1] Sami Alajlouni,[1] Ali Shakouri,[1] and Mahdi Hosseini[1,2,*]

[1]*Birck Nanotechnology Center and Purdue Quantum Science and Engineering Institute, Elmore Family School of Electrical and Computer Engineering, Purdue University, West Lafayette, Indiana 47907, USA*

[2]*Department of Physics and Astronomy, Purdue University, West Lafayette, Indiana 47907, USA*

Optical signals carrying quantum correlations can be used to illuminate objects, enabling, in principle, quantum enhanced sensing of the object or its properties. Here, we demonstrate quantum enhanced temperature sensing of microelectronics using bright quantum optical signals. Relying on lock-in detection of thermoreflectivity, we measure the temperature change of a microwire induced by a current with an accuracy of better than $0.04°$ averaged over 0.1 s. The results show a nearly 50% improvement in accuracy compared to classical light of the same power and is a demonstration of below-shot-noise thermoreflectivity sensing. With moderate improvements, quantum temperature resolution of sub mK can be achieved at optical powers just below the laser-induced heating threshold, and thus the true quantum advantage of temperature sensing is within reach. Other sensing modalities can be adopted to extend the approach to quantum imaging of heat dissipation in microelectronic and semiconductor devices.

I. INTRODUCTION

There is an ever-growing need for better sensing and imaging systems in engineering (e.g. micro- and nanostructure imaging), biology (e.g. single-cell imaging), and fundamental measurements (e.g. gravitational-wave sensing). Optical measurement methods provide a noninvasive and noncontact sensing modality for a wide range of sensing and imaging applications. However, in many cases, the sensitivity of an optical measurement is limited by the shot noise of the illumination light. Using quantum light for illumination can provide means to surpass the shot-noise limit in optical sensing and imaging [1,2]. Applications of quantum light to achieve quantum advantage in displacement sensing [3] and stimulated Raman scattering microscopy [4] have been demonstrated. More specifically, applications of quantum light to enhance sensing have also been suggested in various contents, including imaging [5], lithography [6,7], atomic force microscopy [8], biological imaging [9], phase sensing [10], magnetometry [11], and Brillouin scattering spectroscopy [12]. Quantum-inspired imaging has also attracted interest in the past decade [13–15] given the limitations of quantum light sources.

We explore a different application of bright squeezed states of light generated from a room-temperature source for sensing temperature and heat dissipation in electronic devices. Localized hot spots in electronic devices can significantly reduce device lifetime and performance, thus localized sensing of temperature and imaging heat dissipation in these devices is of great significance [16–18]. Measuring the temperature of micro- and nanoelectronic devices using thermoreflectance measurement has enabled subdiffraction imaging of hot spots in electronic nanostructures [19–22]. By controlling the illumination and detection timing, lock-in detection of thermoreflectivity has achieved 800-ps timing resolution for thermal imaging of cells [23]. Using classical or thermal light, this technique enables shot-noise-limited detection of thermoreflectivity by simultaneously modulating the current in the device and performing impulsive measurements in order to measure a differential signal. A bias current is used to induce a temperature change in a microwire. Due to the nonzero thermoreflectivity coefficient of the metallic wire, this temperature change alters the reflectivity of the wire, which can subsequently be probed by laser light. We demonstrate that lock-in detection of thermoreflectivity using a bright quantum squeezed light can surpass the standard quantum limit in detection of the microwire's temperature.

II. EXPERIMENTAL SETUP

We rely on a technique using lock-in detection of temperature change developed based on classical optical thermoreflectance measurement to sense an aluminum (Al) microwire's temperature. The schematic of our experimental setup is shown in Fig. 1. Bright intensity squeezing

---
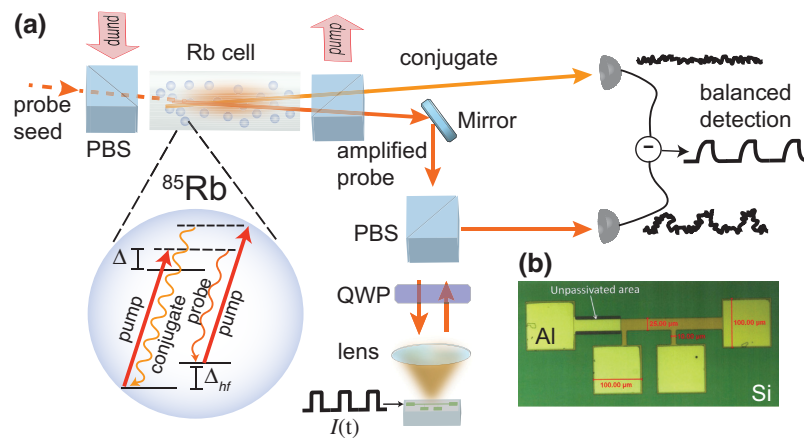
*Corresponding author: mh@purdue.edu

FIG. 1. (a) Schematic of the experimental setup is shown. A polarizing beam splitter (PBS) is used to combine and separate the pump from the squeezed light. The probe passes through a lens and is focused onto the 25-μm-wide aluminum wire. The reflected probe passes through the quarter-wave plate (QWP) again and is reflected toward the balanced detector. The wire is excited by a 50% duty-cycle square wave. The temperature and therefore the reflectivity are modulated with the same frequency, causing this information to be encoded into the intensity of the reflected probe beam. The correlated noise from the conjugate beam is subtracted from the probe beam to produce a low-noise signal that allows us to measure the induced temperature change. (b) An optical microscope image of the Al wire on Si substrate. The area without a protective 200-nm SiN$_x$ layer is referred to as the unpassivated area. This SiN$_x$ layer is placed for environmental protection [24]. The unpassivated area can be used for comparing the thermal effect of the SiN$_x$ layer [25]. The sample has a similar structure as the one in Ref. [25].

is attained in the form of a correlated twin beam generated by four-wave mixing (FWM) inside a ^{85}Rb vapor cell. A Ti:sapphire laser pumps the rubidium atoms, and a probe beam is seeded to give rise to FWM with a double Λ configuration. As a result, the probe beam is amplified and a conjugate beam is generated in the spatial and spectral modes satisfying a phase-matching condition. The photon-number correlation between the Stokes and anti-Stokes photons leads to intensity squeezing between these two beams. The pump is filtered out by a polarizing beam splitter (PBS), and the amplified probe beam propagates toward our Al microwire. The beam is reflected off of the wire and goes to one arm of a single-pixel balanced detector while the conjugate beam goes directly to the other arm of the balanced detector. The current excitation in the microwire leads to a change in temperature and subsequently, a change in the reflectivity of the wire [26]. The current on the wire is modulated to perform lock-in detection and filter out the classical noise in our measurement. This, in turn, produces a modulated reflected probe beam, which contains information about the temperature change of the microwire. The correlated beams are subtracted to achieve noise levels below shot noise and measure the temperature change in the microwire due to the excitation current. As a comparison, we also carry out similar measurements with a twin coherent laser beam (classical light), detected by a balanced detector after one beam reflected off the sample. The lock-in detection and intensity subtraction is carried out the same way as for the quantum light beams to obtain the shot-noise-limited detection sensitivity.

The linearly polarized pump is at a wavelength of 795 nm with 320 mW of power as it enters the 12-mm-long ^{85}Rb vapor cell. The pump is 1.5 GHz blue detuned from the D1 transition ($5^2S_{1/2} \rightarrow 5^2P_{1/2}$) with a resonance at 795 nm. The pump is split before it enters the cell. One of the subsequent beams is directed towards an electro-optic modulator (EOM) to generate a 3.03-GHz frequency shift from the pump frequency, this is our probe beam. After the EOM the carrier light and other unwanted sidebands are filtered using an etalon filter. The probe is then combined with the pump with orthogonal polarization to seed the FWM process. The probe power is 10 μW as it enters the cell. The angle between the pump and probe is set to 5 mrads at which point we observe maximum squeezing between the correlated beams. The vapor cell is heated to 120 °C. With these parameters, the probe is amplified with a gain of 4.3, and a quantum correlated conjugate beam is generated symmetrically with respect to the pump axis. The amplified probe travels to the sample, which is below an aspheric lens ($f = 8$ mm). The aluminium wire is a 25 μm by 300 μm rectangular trace with a theoretically calculated resistance of 6.5Ω. The wire is excited with a current source that produces a square wave with amplitude going from 0 to I_{max}, where I_{max} is varied across different measurements. The frequency of the excitation current is also varied from 10–100 kHz. The reflected probe and conjugate beams are incident on a single-pixel balanced detector with a bandwidth of 1 MHz. The detector subtracts the two beams providing the output used to measure squeezing, change in reflectivity, and subsequently the

temperature sensitivity in our setup. The individual detector signals are also used to find the absolute reflectivity of the wire.

III. EXPERIMENTAL RESULTS

To find the best squeezing, we optimize the experimental parameters (e.g. probe and pump frequency, alignment, temperature, and polarization) while observing the noise in the subtracted signal on a spectrum analyzer after the probe is reflected from the sample. The lens, PBS, and the wire on the probe path after the Rb cell introduce a total loss of about 40% to the probe light limiting the final squeezing to about 3 dB as shown in Fig. 2(a). Correcting for losses in the probe path, the actual squeezing between the generated twin beams is about 7 dB. The optimal regime is between 10–100 kHz. As the detector bandwidth is limited to 1 MHz, squeezing starts to decrease at frequencies > 200 kHz. This gives us the upper and lower bounds for the modulation frequency that we can use to excite the microwire and implement lock-in detection.

Metals experience a change in reflectivity due to changes in temperature, this is called thermoreflectivity. The normalized reflectivity changes with the temperature according to the following relation [25]:

$$\frac{\Delta R}{R} = C_{TR}\Delta T \quad (1)$$

C_{TR} is the thermoreflectivity coefficient. For our experiment, we use an aluminum microwire with a thermoreflectivity coefficient of 1.5×10^{-4} K^{-1} for 795-nm light [27]. When we electrically excite the wire with a current source, the wire's fast thermal response time creates "hot"

and "cold" frames in which the reflectivity is high and low, respectively. The hot and cold frames are observed by the detector's subtracted signal [see Fig. 3(a)]. The response time of the wire is around a few microseconds [see Fig. 3(b)] so we keep the excitation period long enough for the temperature to reach a steady state. To test the limits of temperature sensing in this way, we consider only the change in reflectivity during the steady-state regions and neglect points that are at the hot-cold frame boundaries, since the wire's temperature or current can be unstable at these points.

We subtract the average values of the cold frames from that of the hot frames to do lock-in detection. This process filters out classical noise at frequencies not harmonic to the modulation frequency. Knowing the thermal response time of the wire and the squeezing bandwidth, we can adjust the modulation period and thus the averaging window to perform reflectivity sensing limited by quantum noise. The difference between a single hot-cold frame pair gives a single data point for change in reflectivity, ΔR. Normalizing this value to the dc value of the probe light (R) (without subtraction from the conjugate) gives $\Delta R/R$, which is proportional to the change in temperature of the microwire, ΔT. The variance in this signal across the frames is what we quantify as noise. The total time taken to gather the data, which is the total time for all the frames used to get the signal, is referred to as the measurement time, t_m. To characterize the reflectivity, we repeat the measurement of $\Delta R/R$ for different excitation currents at a particular frequency and plot the data against the current. The results are shown in Fig. 2(b). The data shows a quadratic dependency of reflectivity to current, confirming the fact that the reflectivity changes with the temperature of the wire,
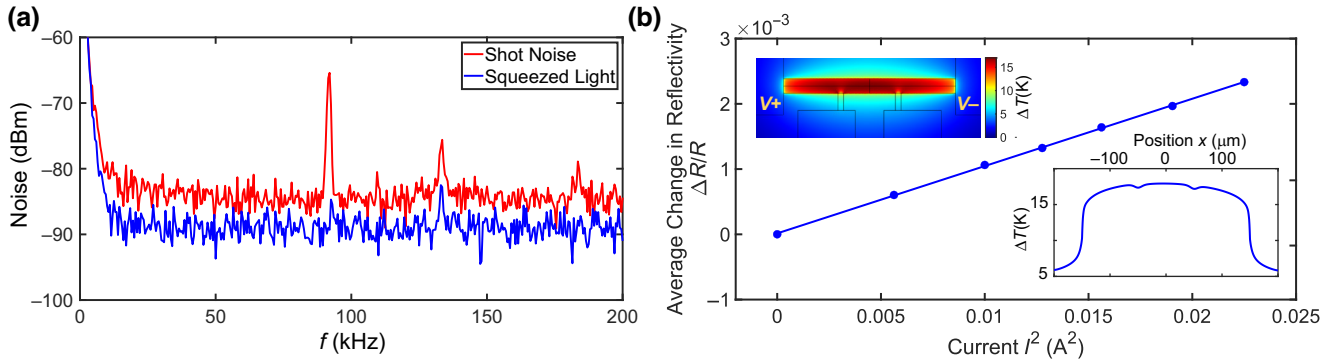

FIG. 2.   (a) The noise comparison of the squeezed quantum light (blue) to classical light (red). We see about 3 dB of squeezing after probe loss by the sample. Maximum squeezing is achieved around $f = 30$ kHz. The noise spikes near 90, 130, and 180 kHz appear to be caused by the noise in the rf signal driving the acousto-optic modulator. (b) The data points represent the signal (average change in reflectivity across frames) with different excitation currents at current modulation frequency $f = 30$ kHz and measurement time $t_m = 50$ ms. The error bars in the data points are smaller than the size of the markers. Our signal changes quadratically with current with a slope of 0.1 A^{-2}. The upper inset shows the theoretical temperature change distribution across the microwire for 150-mA excitation current, which is the last data point in our experimental data curve. The excitation is provided on the far-end pads, as shown. For this temperature change distribution simulation with 150-mA excitation current, the temperature gradient across the length of the wire is shown in the lower inset, where x is the displacement from one end of the wire to the other, with the center being the origin.

which itself follows Ohm's law. Our data also agrees with a finite-element simulation (COMSOL) of the wire's temperature change. With the current setup and corresponding parameter values, we measure squeezing after the probe has been reflected from the sample. Even after additional loss from optics and sample, we still observe about 3 dB of squeezing below the shot noise limit (SNL). The SNL is measured using coherent light with the same total power. Using Eq. (1) we can see that we get ΔT by dividing our normalized signal with the thermoreflectivity constant. The variance, or noise, in the signal dictates the sensitivity of our experiment to variation in the temperature ($\delta(\Delta T)$).

We use this experiment to first study the transient response of the wire by varying the measurement time window and window delay. Figure 3(b) shows the effect of the measurement time window (τ_2), which tells us the measurement time, and its delay with respect to the edge of the current pulse (τ_1) on temperature sensitivity. The delay time of $\tau_1 \simeq 2$ μs marks the transient time scale of temperature and beyond $\tau_1 \simeq 6$ μs the sensitivity remains almost independent of τ_1. The sensitivity is monotonically enhanced with increasing τ_2, which can be seen in Fig. 4(b) as well. At current $I_{max} = 100$ mA, the absolute temperature change from the start to the end of the current pulse is 6.6 K, as confirmed by measurement of absolute change in reflectivity as well as finite-element simulation. The temperature sensitivity of 0.14 K during the transient time is below the absolute temperature change and suggests that quantum light can be used to study the transient response of the wire with better accuracy compared to classical light. From this analysis, we have a better estimate of

the response time of the wire. We see that wire begins to achieve steady-state after 4 μs. We continue with the rest of our analysis by keeping the time window and window delay as what we determined from this plot.

After identifying the detection times τ_1 and τ_2, we test the sensitivity of the measurement to the current's modulation frequency. Figure 4(a) shows temperature sensitivity as a function of modulation frequency. The quantum sensitivity is fairly constant across the measured frequency. This is expected as the quantum noise, as seen in Fig. 2(a), is constant over this frequency range. Although the SNR and the gap between quantum and classical noise is highest at around 10 kHz, we are more concerned with achieving better sensitivity, which is best achieved at 30 kHz given the trade-off between the wire's thermal response time, squeezing spectrum, and the detector's bandwidth. As can be seen in Fig. 2(a), the absolute noise level is higher at 10 kHz due to the excess classical noise. Hence, the difference in quantum and classical SNR plotted in the inset of Fig. 4(a) is larger at 10 kHZ. However, the temperature sensitivity observed is higher at 30 kHz, because the absolute noise level is lower. Moreover, at 10 kHz our classical measurement is not shot noise limited due to the excess classical noise at low frequencies. Looking at this analysis, the following experimental results are obtained at a fixed modulation frequency of $f = 30$ kHz.

Temperature sensitivity improves with increasing the measurement time, t_m [see Fig. 4(b)]. Both classical and quantum light show the same scaling within a time of $1/\sqrt{t_m}$, while quantum measurements have a scaling factor of 2/3. The classical light in our case is the difference between two twin coherent laser beams, not generated
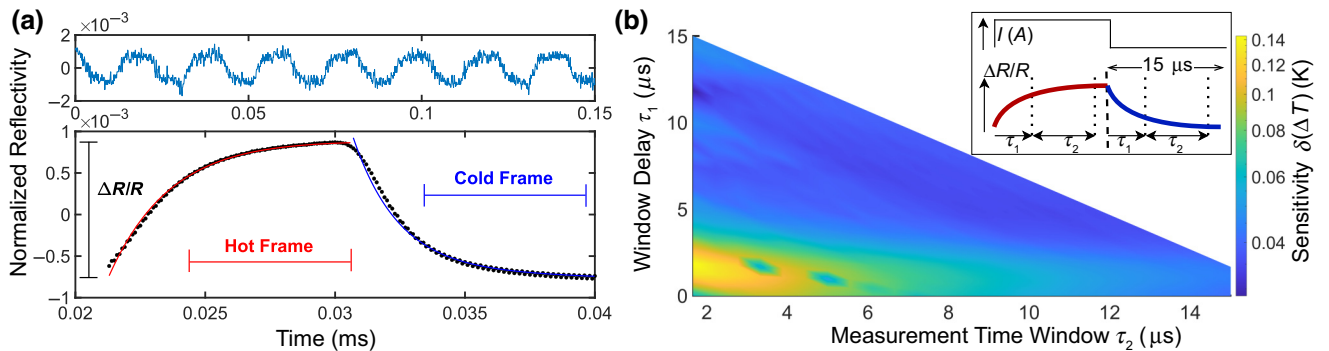

FIG. 3. (a) The upper plot shows the raw differential signal detected for measurement with an excitation current of 113 mA modulated at a frequency of 50 kHz. This signal is produced by subtracting the conjugate beam from the probe beam to eliminate the correlated noise in the twin beams. The signal is normalized to the absolute probe-beam intensity. The lower plot is an enlarged version of the upper plot depicting a pair of heating and cooling intervals, averaged over many intervals. The indicated hot and cold frames are of equal length and capture steady-state information. The transient heating and cooling behaviors are modeled by a double exponential function shown by solid red and blue lines, respectively. (b) The sensitivity of temperature measurement is shown as a function of the measurement time window, τ_2, and its delay with respect to the edge of the current pulse, τ_1. The total length is limited by the pulse duration and hence the plot has a diagonal boundary. For this experiment, we use an excitation current, $I = 100$ mA, modulation frequency, $f = 30$ kHz, and measurement time, $t_m = 50$ ms. The inset shows the schematic of a current pulse and the corresponding reflectivity marking τ_1 and τ_2 times.
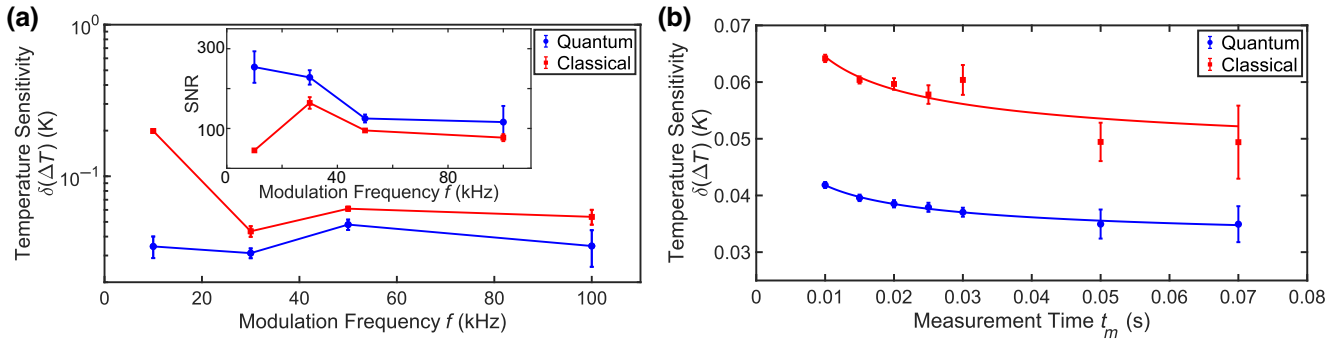
FIG. 4. (a) The plot presents a comparison of the temperature sensitivity of quantum and classical light as a function of the current modulation frequency. The excitation current is set to $I_{\text{max}} = 100$ mA with a measurement time of $t_m = 50$ ms. The inset shows a comparison of the SNR of the two regimes, also done for $I_{\text{max}} = 100$ mA and $t_m = 50$ ms. Using quantum correlated light, we obtain a SNR of about 225 at 30 kHz. (b) The graph shows the temperature sensitivity plotted against the measurement time. The quantum correlated light results in a temperature sensitivity that is 1.5 times better than classical light. We have larger error bars for higher t_m values due to the undersampling in the measurement given the total measurement time fixed at 100 ms. The data points are fitted with a $1/\sqrt{t_m}$ fit, weighted by the error bars. Other experimental parameters include $f = 30$ kHz and $I_{\text{max}} = 100$ mA. We are able to achieve a sensitivity of about 35 ± 3 mK after a measurement time of 50 ms. For the data points at a lower t_m, the size of the error bars is smaller than the marker size.

through FWM. The larger error bars at long measurement times are the result of undersampling given the total acquisition time of 800 ms for all data points.

IV. DISCUSSION

Although our results show enhanced temperature sensing using quantum correlated light when compared to classical light (a twin coherent beam), the question is if such an enhancement can be offset by using stronger classical light. Our finite-element simulation shows that increasing the laser probe power to about 1 mW will cause laser-induced heating, locally increasing the temperature of the wire, by about 0.5 K. This is comparable to, or larger than, the minimum current-induced heating that we can measure. In our experiment, the probe and conjugate power is limited by the laser power and detector saturation limit. However, this can be avoided by moderate modification of the experiments to obtain and measure squeezing at mW probe powers. We note that squeezing of 9.2 dB was already demonstrated in a similar system using 1.2 W of pump power and > 2 mW of probe power [28]. Using state-of-the-art squeezing results, we expect a sub-mK temperature sensitivity after a measurement time of just 0.1 s and using a probe power of 2 mW. In this regime, quantum temperature sensing can be achieved beyond the laser-heating limit, suggesting that the quantum advantage of temperature sensing in microelectronics is within reach.

Moreover, raster scanning a quantum probe across the sample can result in obtaining thermal quantum images to study heat dissipation and diffusion on small scales. The single-pixel detectors are fast enough to observe squeezing and when combined with fast probe scanning, they can enable quantum imaging without the need for high-speed

EMCCD cameras. Applications of single-pixel detectors for imaging in the classical regime have been demonstrated in various contexts [29–33]. In the quantum regime, however, any loss is detrimental to the quantum signal and most imaging techniques by definition rely on partial loss of light to image objects. Quantum imaging of thermoreflectivity can be realized if the reflectivity or transmissivity of the sample is high across the region being imaged. Within the metallic regions where reflectivity is high, temperature gradients can be imaged with high accuracy to determine the spatial thermal response to a radio-frequency drive. In the case of the semiconductor substrate, a thin layer of dielectric can be deposited to perform quantum thermoreflective imaging, albeit evasively, to accurately study heat dissipation in low-power electronic devices.

V. CONCLUSION

In conclusion, we generate quantum correlated twin beams of light using a seeded four-wave mixing process in ^{85}Rb, and apply this to thermoreflective sensing. We rely on quantum correlations of the illumination light, lock-in detection of reflectivity, and the thermoreflectivity effect in electronic structures to sense reflectivity (or temperature) change in a microwire. We obtain a temperature sensitivity of about 35 mK after averaging for just 50 ms. Our results show an improvement of a factor of 1.5 when compared to sensing with coherent light or shot noise. Moderate changes to the experiment, including using a higher-power laser may enable temperature sensitivity in the microkelvin regime for mW-power quantum light where classical sensitivity can no longer be increased by increasing light power. This is because the laser-induced heating in this regime

can be comparable to, or higher than, the current-induced temperature change.

Going forward, integrating multimode quantum light sources such as FWM sources, lock-in detection techniques, and image-processing algorithms can help to identify and implement practical advantages in quantum sensing and imaging applied to semiconductor technology. In principle, quantum imaging can be achieved using multimode light [34] and high-speed EMCCD cameras [35], or by raster scanning the probe beam and using single-pixel detectors [29].

[1] P.-A. Moreau, E. Toninelli, T. Gregory, and M. Padgett, Imaging with quantum states of light, Nat. Rev. Phys. **1,** 1 (2019).

[2] S. Pirandola, B. Bardhan, T. Gehring, C. Weedbrook, and S. Lloyd, Advances in photonic quantum sensing, Nat. Photon. **12,** 724 (2018).

[3] J. Aasi, J. Abadie, B. Abbott, R. Abbott, T. Abbott, M. Abernathy, C. Adams, T. Adams, P. Addesso, R. Adhikari, C. Affeldt, O. Aguiar, P. Ajith, B. Allen, E. Ceron, D. Amariutei, S. Anderson, W. Anderson, K. Arai, and J. Zweizig, Enhanced sensitivity of the LIGO gravitational wave detector by using squeezed states of light, Nat. Photon. **7,** 613 (2013).

[4] C. Casacio, L. Madsen, A. Terrasson, M. Waleed, K. Barnscheidt, B. Hage, M. Taylor, and W. Bowen, Quantum-enhanced nonlinear microscopy, Nature **594,** 201 (2021).

[5] J. Clark, Z. Zhou, Q. Glorieux, A. Marino, P. Lett, M. Marino, and K. Jones, Imaging using quantum noise properties of light, Opt. Express **20,** 17050 (2012).

[6] J. P. Dowling, Quantum optical metrology – the lowdown on high-n00n states, Contemp. Phys. **49,** 125 (2008).

[7] A. N. Boto, P. Kok, D. S. Abrams, S. L. Braunstein, C. P. Williams, and J. P. Dowling, Quantum Interferometric Optical Lithography: Exploiting Entanglement to Beat the Diffraction Limit, Phys. Rev. Lett. **85,** 2733 (2000).

[8] R. C. Pooser, N. Savino, E. Batson, J. L. Beckey, J. Garcia, and B. J. Lawrie, Truncated Nonlinear Interferometry for Quantum-Enhanced Atomic Force Microscopy, Phys. Rev. Lett. **124,** 230504 (2020).

[9] M. A. Taylor, J. Janousek, V. Daria, J. Knittel, B. Hage, H.-A. Bachor, and W. P. Bowen, Subdiffraction-Limited Quantum Imaging Within a Living Cell, Phys. Rev. X **4,** 011017 (2014).

[10] B. Anderson, P. Gupta, B. Schmittberger, T. Horrom, C. Hermann Avigliano, K. Jones, and P. Lett, Phase sensing beyond the standard quantum limit with a truncated Su(1,1) interferometer, Optica **4,** 752 (2016).

[11] N. Otterstrom, R. Pooser, and B. Lawrie, Nonlinear optical magnetometry with accessible *in situ* optical squeezing, Opt. Lett. **39,** 6533 (2014).

[12] V. Yakovlev, T. Li, F. Li, X. Liu, and G. Agarwal, Quantum-enhanced stimulated Brillouin scattering spectroscopy and imaging, Optica **9,** 959 (2022).

[13] A. Kirmani, D. Venkatraman, D. Shin, A. Colaço, F. N. C. Wong, J. H. Shapiro, and V. K. Goyal, First-photon imaging, Science **343,** 58 (2014).

[14] J. Shapiro, D. Venkatraman, and F. Wong, Ghost imaging without discord, Sci. Rep. **3,** 1849 (2013).

[15] F. Guerrieri, L. Maccone, F. N. C. Wong, J. H. Shapiro, S. Tisa, and F. Zappa, Sub-Rayleigh Imaging via *n*-Photon Detection, Phys. Rev. Lett. **105,** 163602 (2010).

[16] P. K. Chundi, Y. Zhou, M. Kim, E. Kursun, and M. Seok, in *2017 IEEE/ACM International Symposium on Low Power Electronics and Design (ISLPED)* (2017), p. 1.

[17] T. Ghanbari, Hot spot detection and prevention using a simple method in photovoltaic panels, IET Gen. Transm. Distribution **11,** 883 (2017).

[18] Y. M. Banadaki, A. Srivastava, and S. Sharifi, in *Nanosensors, Biosensors, and Info-Tech Sensors and Systems 2016,* Vol. 9802, edited by V. K. Varadan, International Society for Optics and Photonics (SPIE, 2016), p. 980203.

[19] A. Ziabari, M. Parsa, Y. Xuan, J.-H. Bahk, K. Yazawa, F. X. Alvarez, and A. Shakouri, Far-field thermal imaging below diffraction limit, Opt. Express **28,** 7036 (2020).

[20] K. Maize, S. R. Das, S. Sadeque, A. M. S. Mohammed, A. Shakouri, D. B. Janes, and M. A. Alam, Super-joule heating in graphene and silver nanowire network, Appl. Phys. Lett. **106,** 143104 (2015).

[21] T. Favaloro, J. Suh, B. Vermeersch, K. Liu, Y. Gu, L.-Q. Chen, K. X. Wang, J. Wu, and A. Shakouri, Direct observation of nanoscale Peltier and joule effects at metal–insulator domain walls in vanadium dioxide nanobeams, Nano Lett. **14,** 2394 (2014). pMID: 24735496,

[22] S. Shin, M. A. Wahab, M. Masuduzzaman, K. Maize, J. Gu, M. Si, A. Shakouri, P. D. Ye, and M. A. Alam, Direct observation of self-heating in III–V gate-all-around nanowire MOSFETs, IEEE Trans. Electron. Devices **62,** 3516 (2015).

[23] Y. Bai, D. Zhang, L. Lan, Y. Huang, K. Maize, A. Shakouri, and J.-X. Cheng, Ultrafast chemical imaging by widefield photothermal sensing of infrared absorption, Sci. Adv. **5,** eaav7127 (2019).

[24] B. Vermeersch, J.-H. Bahk, J. Christofferson, and A. Shakouri, Thermoreflectance imaging of sub 100 ns pulsed cooling in high-speed thermoelectric microcoolers, J. Appl. Phys. **113,** 104502 (2013).

[25] T. Favaloro, J.-H. Bahk, and A. Shakouri, Characterization of the temperature dependence of the thermoreflectance coefficient for conductive thin films, Rev. Sci. Instrum. **86,** 024903 (2015).

[26] *Picosecond Transient Thermal Imaging Using a CCD Based Thermoreflectance System,* International Heat Transfer Conference, Vol. 2010 14th International Heat Transfer Conference, Volume 4 (2010).

[27] P. E. Raad, P. L. Komarov, and M. G. Burzo, Technical brief: Thermo-reflectance thermography for submicron temperature measurements, Electron. Cooling **14,** 28 (2008).

[28] Q. Glorieux, L. Guidoni, S. Guibal, J.-P. Likforman, and T. Coudreau, Quantum correlations by four-wave mixing in an atomic vapor in a nonamplifying regime: Quantum beam splitter for photons, Phys. Rev. A **84**, 053826 (2011).

[29] G. M. Gibson, S. D. Johnson, and M. J. Padgett, Single-pixel imaging 12 years on: A review, Opt. Express **28**, 28190 (2020).

[30] P. Sen, B. Chen, G. Garg, S. R. Marschner, M. Horowitz, M. Levoy, and H. P. A. Lensch, Dual photography, ACM Trans. Graph. **24**, 745 (2005).

[31] J. Greenberg, K. Krishnamurthy, and D. Brady, Compressive single-pixel snapshot x-ray diffraction imaging, Opt. Lett. **39**, 111 (2014).

[32] W. L. Chan, K. Charan, D. Takhar, K. F. Kelly, R. G. Baraniuk, and D. M. Mittleman, A single-pixel terahertz imaging system based on compressed sensing, Appl. Phys. Lett. **93**, 121105 (2008).

[33] V. Studer, J. Bobin, M. Chahid, H. S. Mousavi, E. Candes, and M. Dahan, Compressive fluorescence microscopy for biological and hyperspectral imaging, Proc. Nat. Acad. Sci. **109**, E1679 (2012).

[34] R. Yang, J. Zhang, I. Klich, C. González-Arciniegas, and O. Pfister, and Spatiotemporal graph states from a single optical parametric oscillator, Phys. Rev. A **101**, 043832 (2020).

[35] E. S. Matekole, S. L. Cuozzo, N. Prajapati, N. Bhusal, H. Lee, I. Novikova, E. E. Mikhailov, J. P. Dowling, and L. Cohen, Quantum-Limited Squeezed Light Detection with a Camera, Phys. Rev. Lett. **125**, 113602 (2020).